Targeting atherosclerosis by using modular, multifunctional micelles

David Peters[a,b], Mark Kastantin[c], Venkata Ramana Kotamraju[a], Priya P. Karmali[d], Kunal Gujraty[a], Matthew Tirrell[c], and Erkki Ruoslahti[a,d,1]

[a]Vascular Mapping Center, Burnham Institute for Medical Research, University of California, Santa Barbara, 3119 Biology II Building, CA 93106-9610; [b]Biomedical Sciences Graduate Group, University of California at San Diego, La Jolla, CA 92037; [c]Department of Chemical Engineering, University of California, Santa Barbara, CA 93106-5080; and [d]Cancer Research Center, Burnham Institute for Medical Research, 10901 North Torrey Pines Road, La Jolla, CA 92037-1005

Contributed by Erkki Ruoslahti, March 26, 2009 (sent for review December 6, 2008)

Subtle clotting that occurs on the luminal surface of atherosclerotic plaques presents a novel target for nanoparticle-based diagnostics and therapeutics. We have developed modular multifunctional micelles that contain a targeting element, a fluorophore, and, when desired, a drug component in the same particle. Targeting atherosclerotic plaques in ApoE-null mice fed a high-fat diet was accomplished with the pentapeptide cysteine-arginine-glutamic acid-lysine-alanine, which binds to clotted plasma proteins. The fluorescent micelles bind to the entire surface of the plaque, and notably, concentrate at the shoulders of the plaque, a location that is prone to rupture. We also show that the targeted micelles deliver an increased concentration of the anticoagulant drug hirulog to the plaque compared with untargeted micelles.

cysteine-arginine-glutamic acid-lysine-alanine | hirulog | plaque | imaging | nanoparicles

Cardiovascular disease affects 1 in 3 people in the United States during their lifetime, and accounts for nearly a third of the deaths that occur each year (1). Atherosclerosis is one of the leading causes of cardiovascular disease, and it results in raised plaques in the arterial wall that can occlude the vascular lumen and block blood flow through the vessel. Recently, it has become clear that not all plaques are the same. Those susceptible to rupture, fissuring, and subsequent thrombosis are most frequently the cause of acute coronary syndromes and death (2).

Rupture of an atherosclerotic plaque exposes collagen and other plaque components to the bloodstream. This rupture initiates hemostasis in the blood vessel and leads to activation of thrombin and a thrombus to form at the site of rupture. Elevated levels of activated thrombin bound to the vessel wall have been observed up to 72 h after vascular injury (3). These elevated thrombin levels not only induce clot formation but also have been implicated in the progression of atherosclerosis by causing smooth muscle cells to bind circulating low density lipoprotein (4). Subtle clotting in plaques is also indicated by deposition of fibrin(ogen) both inside and on the surface of atherosclerotic plaques, which has been well documented since the 1940s (5–7).

Fibrin-containing blood clots have been extensively used as a target for site-specific delivery of imaging agents and anticlotting agents to thrombi (8–10). Delivering anticoagulants into vessels where clotting is taking place has been shown to be effective at reducing the formation and expansion of clots, and it also decreases the risk of systemic side effects (11, 12). Antibodies and peptides that bind to molecular markers specifically expressed on atherosclerotic plaques have shown promise for plaque imaging in vivo (13–16), but clotting on the plaque has not been used as a target. We reasoned that the fibrin deposited on plaques could serve as a target for delivering diagnostic and therapeutic compounds to plaques.

We chose the clot-binding peptide cysteine-arginine-glutamic acid-lysine-alanine (CREKA) to test the suitability of fibrin (clotted plasma proteins) for plaque targeting. This peptide was identified as a tumor-homing peptide by in vivo phage library screening, and subsequently it was shown to bind to clotted plasma proteins in the blood vessels and stroma of tumors (17, 18). Here, we show that CREKA-targeted micelles can be used to deliver and concentrate imaging dyes and the direct thrombin inhibitor hirulog in atherosclerotic plaques in the ApoE-null mouse model in vivo.

Results

Modular Multifunctional Micelles. The general structure of the micelles is shown in Fig. 1. We designed individual lipopeptide monomers with a 1,2-distearoyl-*sn*-glycero-3-phosphoethanolamine (DSPE) tail, a PEG_{2000} spacer, and a variable head group, which was the carboxyfluorescein (FAM)-CREKA peptide, an infrared fluorophor, or the hirulog peptide. When placed in aqueous solution, these compounds formed micelles with an average hydrodynamic diameter of 17.0 ± 1.0 nm. We made targeted micelles from the FAM-CREKA monomers alone, or by mixing all 3 monomers together. Nontargeted control micelles were obtained by mixing FAM-labeled monomers with *N*-acetylcysteine monomers. Half-life of FAM-CREKA micelles and CREKA/hirulog mixed micelles in circulation was determined by fluorescence, and was 130 and 100 min, respectively.

Ex Vivo Imaging of the Aortic Tree in Atherosclerotic Mice. We induced atherosclerotic plaques in ApoE-null mice by keeping them on a high-fat diet (19, 20). Earlier studies have revealed fibrin accumulation at the surface and interior of atherosclerotic plaques in other animal models and on human plaques (21). We obtained similar results in the ApoE model; anti-fibrin(ogen) antibodies stained the plaques, but not the normal-appearing vessel wall in this model (see Fig. 3*A Bottom*), indicating the presence of clotted plasma proteins at these sites. To determine whether these fibrin(ogen) deposits could serve as a target for imaging, we injected fluorescein-labeled CREKA micelles into these mice and imaged the isolated aortic tree ex vivo. High fluorescence intensity was observed in the regions that contained most of the atherosclerotic lesions. In the ApoE-null mouse, these regions include the brachiocephalic artery and the lower aortic arch (22). Quantitative comparison with fluorescent nontargeted micelles revealed a large difference between the micelles that were targeted (fluorescence intensity in arbitrary units: 209,000 ± 59,000) and those not targeted (5,100 ± 3,300; Fig. 2). The difference was statistically significant ($P \leq 0.05$).

Author contributions: D.P., M.T., and E.R. designed research; D.P., M.K., P.P.K., and K.G. performed research; M.K. and V.R.K. contributed new reagents/analytic tools; D.P. analyzed data; and D.P. and E.R. wrote the paper.

The authors declare no conflict of interest.

Freely available online through the PNAS open access option.

[1]To whom correspondence should be addressed. E-mail: ruoslahti@burnham.org.

This article contains supporting information online at www.pnas.org/cgi/content/full/0903369106/DCSupplemental.

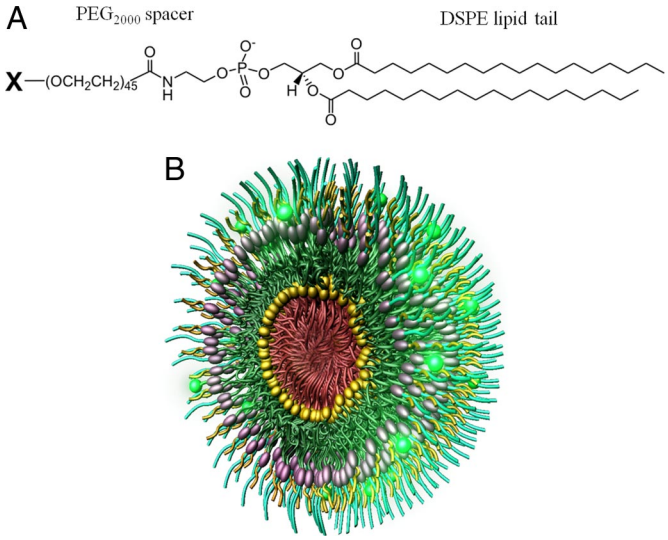

Fig. 1. Construction of modular multifunctional micelles. (*A*) Individual lipopeptide monomers are made up of a DSPE tail, a poly(ethylene glycol) (PEG_{2000}) spacer, and a variable polar head group (X) of CREKA, FAM-CREKA, FAM, *N*-acetylcysteine, Cy7, or hirulog. The monomers were combined to form various mixed micelles. (*B*) The 3D structure of FAM-CREKA/Cy7/hirulog mixed micelle.

The fluorescence in the aortic tree from the CREKA-targeted micelles was abolished when an excess of unlabeled CREKA micelles was preinjected (5,200 ± 4,800; $P \leq 0.05$), whereas unlabeled, nontargeted micelles did not significantly inhibit the CREKA micelle homing (163,000 ± 34,000). These results indicate that CREKA micelles are able to specifically target the diseased vasculature in atherosclerotic mice and concentrate in areas that are prone to atherosclerotic plaque formation.

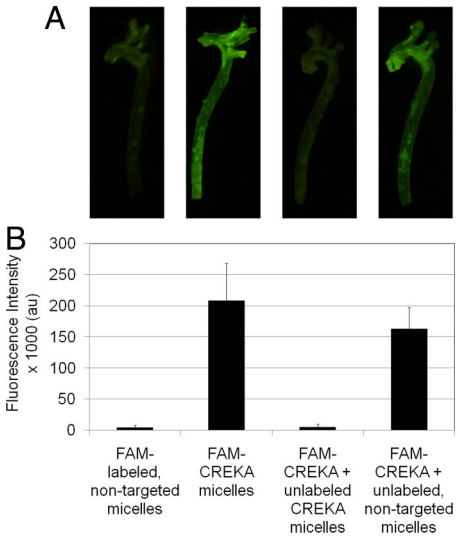

Fig. 2. Ex vivo imaging of the aortic tree of atherosclerotic mice. Micelles were injected intravenously and allowed to circulate for 3 h. The aortic tree was excised after perfusion and imaged ex vivo. (*A*) (Images correspond to the bars directly below them in *B*). Increased fluorescence was observed in the aortic tree of ApoE-null mice after injection with FAM-CREKA targeted micelles, but not with nontargeted fluorescent micelles. When an excess of unlabeled CREKA micelles was injected before the FAM-CREKA micelles, fluorescence in the aortic tree was decreased. A preinjection of an excess of nontargeted unlabeled micelles did not cause a significant decrease in fluorescence. (*B*) Fluorescence in the aortic tree was quantified by measuring the intensity (au, arbitrary units) of fluorescent pixels ($n = 3$ per group).

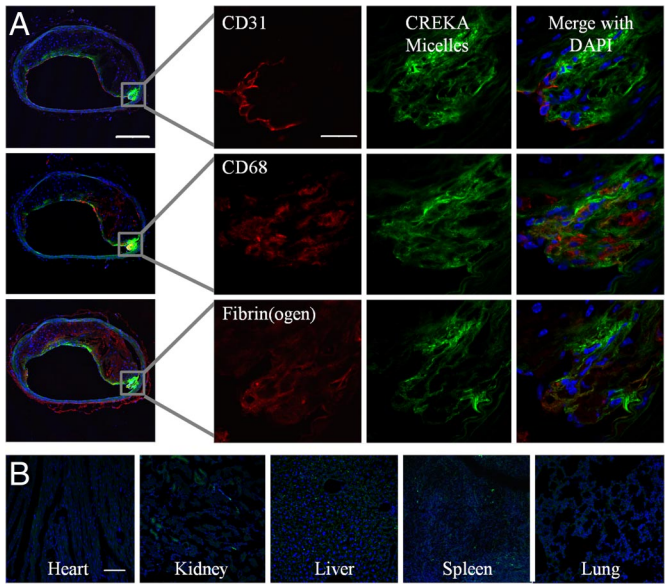

Fig. 3. Localization of CREKA micelles in atherosclerotic plaques. (*A*) Serial cross-sections (5 μm thick) were stained with antibodies against CD31 (endothelial cells; *Top*), CD68 (macrophages and other lymphocytes; *Middle*), and fibrin(ogen) (*Bottom*). Representative microscopic fields are shown to illustrate the localization of micelle nanoparticles in the atherosclerotic plaque. Micelles are bound to the entire surface of the plaque with no apparent binding to the healthy portion of the vessel. CREKA targeted micelles also penetrate under the endothelial layer (CD31 staining) in the shoulder of the plaque (*Inset*) where there is high inflammation (CD68 staining) and the plaque is prone to rupture. Clotted plasma proteins are seen throughout the plaque and its surface [fibrin(ogen) staining]. (*Left*) Images were taken at a 10× magnification. (Scale bar, 200 μm.) (*Right*) Images were taken at a 150× magnification. (Scale bar, 20 μm.) (*B*) Fluorescence was not observed in the heart or lung, and only a small amount was seen in the kidney, spleen, and liver. Images were taken at a 20× magnification. (Scale bar, 100 μm.)

Binding of CREKA Micelles to Atherosclerotic Plaques. Histological examination of the vascular tree from mice injected with CREKA micelles revealed fluorescence on the luminal surface of plaques, whereas there was no significant binding to the histologically healthy portion of the blood vessel in microscopic cross-sections (Fig. 3*A*). Strikingly, the micelles appeared to concentrate in the shoulder regions of the plaque (Fig. 3*A Insets*) where plaques are known to be prone to rupture (23, 24). Fluorescence from the micelles was seen underneath the endothelial layer in the plaque in areas of high inflammation as shown with anti-CD31 (endothelial cells) and anti-CD68 (macrophages and lymphocytes) immunofluorescence. Clotted plasma proteins were visualized on the surface of and throughout the interior of the plaque when anti-fibrinogen antibodies were used. CREKA micelles did not bind substantially to other tissues, including the heart and lungs, but small quantities were found in the liver, spleen, and kidneys, tissues known to nonspecifically trap nanoparticles (Fig. 3*B*). Also, there was no accumulation of CREKA micelles in the aortas of normal mice (Fig. S1). Thus, CREKA micelles specifically target atherosclerotic plaques, concentrating in areas that are prone to rupture with no appreciable binding to healthy vasculature.

Role of Clotting in Binding of CREKA Micelles to Atherosclerotic Plaques. Binding of CREKA iron oxide nanoparticles to tumor vessels has previously been shown to induce clotting in the lumen of these vessels and amplify the binding of the particles (15). The tumor homing of the CREKA iron oxide particles was greatly reduced in that study by preinjecting heparin, which prevented the clotting-induced amplification. The clotting-mediated am-

plification, although potentially beneficial in the diagnosis and treatment of cancer, would not be desirable in the management of atherosclerosis. No clotting was observed in the lumen of atherosclerotic blood vessels in microscopic cross-sections after injection of CREKA micelles. High fluorescence intensity was also still observed in the aortas of atherosclerotic mice injected with FAM-CREKA micelles after a preinjection of heparin (Fig. S2*A*). To determine whether the absence of induction of clotting by CREKA at the plaque surface was a characteristic of the micelles or the plaque microenvironment, we injected CREKA micelles into mice bearing 22Rv1 tumors in which CREKA iron oxide nanoparticles cause intravascular clotting. CREKA micelles accumulated at the walls of tumor vessels but caused no detectable intravascular clotting (Fig. S2*B*). Also, clotting time of normal plasma in the presence of CREKA micelles as measured by using a thrombelastography assay did not change significantly from that of normal plasma alone (21.1 ± 0.7 and 20.2 ± 2.0 min, respectively). However, clotting times of normal plasma in the presence of CREKA iron oxide particles were significantly decreased in the assay (12.3 ± 0.5 min; $P \leq 0.001$). Thus, unlike CREKA iron oxide particles (1), CREKA micelles do not seem to induce clotting in the target vessels or decrease the clotting time in a thrombelastography assay, suggesting that the CREKA micellar platform is suitable for nanoparticle targeting to atherosclerotic plaques.

Targeting of the Antithrombin Peptide Hirulog to Atherosclerotic Plaques. The anticoagulant heparin is used in patients with unstable angina to prevent further clots from forming. However, this drug inhibits thrombin indirectly, and it cannot inhibit the thrombin that is already bound to fibrin. Also, its use can also lead to serious complications, including major bleeding events and thrombocytopenia. Direct thrombin inhibitors have fewer side effects and can inhibit thrombin that is already bound to a blood clot. Hirulog is a small synthetic peptide that was designed by combining the active sites from the natural thrombin inhibitor hirudin through a flexible glycine linker into a single 20-amino acid peptide (23). We conjugated this peptide onto our micellar nanoparticles and showed that it retains full activity in a chromogenic assay for thrombin activity (Fig. 4*A*). We next sought to use CREKA targeted micelles to deliver hirulog to atherosclerotic plaques. CREKA/FAM/hirulog mixed micelles were injected into atherosclerotic mice and allowed to circulate for 3 h. The accumulation of fluorescence in atherosclerotic aortas was identical to that of CREKA/FAM micelles described above. Antithrombin activity in the excised aortic tree was significantly higher in the aortas of mice injected with CREKA targeted micelles than in mice that received nontargeted micelles (1.8 and 1.2 μg/mg of tissue; $P \leq 0.05$). CREKA targeted micelles also caused significantly higher antithrombin activity in the aortas of atherosclerotic than wild-type mice (0.8 μg/mg of tissue; $P \leq 0.05$; Fig. 4*B*). Thus, CREKA targeted micelles seem to selectively deliver hirulog to plaques.

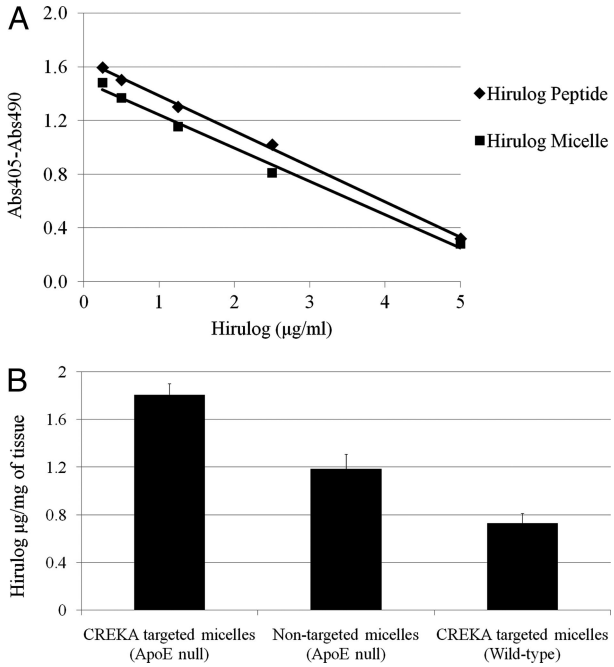

Fig. 4. Targeting of hirulog to atherosclerotic plaques. (*A*) Equal molar concentrations of hirulog peptide and hirulog micelles were tested for antithrombin activity to ensure that potency did not decrease when hirulog was in micellar form. Hirulog peptide and micelles showed similar activity in a chromogenic assay. (*B*) CREKA targeted or nontargeted and hirulog mixed micelles were injected intravenously into mice and allowed to circulate for 3 h. The aortic tree was excised and analyzed for bound hirulog. Significantly higher levels of antithrombin activity were observed in the aortic tree of ApoE-null mice after injection of CREKA targeted hirulog micelles than nontargeted micelles (1.8 and 1.2 μg/mg of tissue; $P \leq 0.05$; $n = 3$). Antithrombin activity generated by CREKA targeted hirulog micelles in ApoE-null mice was also significantly higher than that in wild-type mice (0.8 μg/mg of tissue; $P \leq 0.05$; $n = 3$).

Discussion

We describe the use of targeted micellar nanoparticles to direct both diagnostic imaging dyes and a therapeutic compound to atherosclerotic plaques in vivo. Mixed micelles composed of lipid-tailed clot-binding peptide CREKA as a targeting element, a fluorescent dye as a labeling agent, and, in some cases, hirulog as an anticoagulant specifically bound to plaques. The plaques accumulated fluorescence, and, when hirulog was included in the micelles, an increased level of antithrombin activity was seen in the diseased vessels. The modularity that is inherent to our micellar nanoparticle platform allows multiple functions to be built into the nanoparticle.

Micelles coated with the CREKA peptide were able to specifically target diseased vasculature in ApoE-null mice. The specificity of the targeting was evident from a number of observations. First, fluorescence from the micelles in the aortic tree of atherosclerotic mice localized to known areas of plaque formation, and no fluorescence was observed in wild-type mice. Second, CREKA micelles bind to the entire surface of the plaque in histological sections but do not bind to the healthy portion of the vessel. Third, an excess of unlabeled CREKA micelles inhibited the plaque binding of fluorescent CREKA micelles. Thus, micelles targeted with the CREKA peptide present a potentially useful approach to targeting atherosclerotic plaques.

Although the CREKA micelles decorated the entire surface of plaques, the strongest accumulation of the micelles was at the shoulder, the junction between the plaque and the histologically healthy portion of the vessel wall, which is the site most prone to rupture (22). The high concentration of targeted micelles in the lesion shoulder suggests that these micelles may be effective in delivering compounds to rupture-prone plaques.

Increased fluorescence was observed in the aortic tree of atherosclerotic mice after injection of fluorescent CREKA micelles in imaging. We also examined the feasibility of imaging atherosclerotic plaques in intact animals. Unfortunately, CREKA micelles labeled with the infrared dye Cy7 did not produce a sufficient signal to visualize the plaques in vivo, presumably because of insufficient tissue penetration of the exciting and emitted signals. The modularity of the micelles allows the construction of probes for more sensitive and penetrating imaging techniques, such as PET or MRI.

The homing of CREKA-coated iron-oxide nanoparticles to tumors partially depends on blood clotting induced by the particles within tumor vessels (2). Importantly, CREKA micelles appear to be less thrombogenic than CREKA-coated iron oxide nanoparticles, because the micelles, although homing to tumor vessels, did not induce any detectable additional clotting in them, and they did not reduce clotting times in a thrombelastography assay. Also, inhibiting blood clotting in atherosclerotic mice with heparin had no significant effect on the accumulation of CREKA micelles in the plaques. Thus, the thrombogenicity of CREKA micelles is low, and they appear to target only preformed clotted material in both tumors and plaques.

Because the presence of the anticoagulant heparin did not significantly reduce CREKA micelle targeting to plaques, we were able to use CREKA micelles to deliver an anticoagulant to these lesions. Like CREKA/FAM micelles, CREKA/hirulog mixed micelles accumulated in the rupture-prone shoulder regions of plaques and significantly increased antithrombin activity in the diseased vasculature. Thus, the CREKA micelle platform may be useful in reducing the clotting tendency in plaques and could potentially also reduce the risk of thrombus formation on plaque rupture. Also, the targeting makes it possible to lower the dose, which should reduce the risk of bleeding complications.

Materials and Methods

Micelles. The anticoagulant peptide hirulog-2 was modified by adding a cysteine residue to the N terminus [Cys-D-Phe-Pro-Arg-Pro-$(Gly)_4$-Asn-Gly-Asp-Phe-Glu-Glu-Ile-Pro-Glu-Glu-Tyr-Leu] for covalent conjugation to the micelle lipid tail. Synthesis of all of the peptides was performed by adapting Fmoc/t-Bu strategy on a microwave-assisted automated peptide synthesizer (Liberty; CEM). Peptide crude mixtures were purified by HPLC using 0.1% trifluoroacetic acid in acetonitrile/water mixtures. The peptides obtained were 90–95% pure by HPLC, and were characterized by Q-TOF mass spectral analysis.

DSPE-PEG_{2000}-maleimide and DSPE-PEG_{2000}-amine were purchased from Avanti Polar Lipids. Cy7 mono-*N*-hydroxysuccinimide ester was purchased from Amersham Biosciences.

Cysteine-containing peptides were conjugated via a thioether linkage to DSPE-PEG_{2000}-maleimide by adding a 10% molar excess of the lipid to a water/methanol solution (90:10, vol/vol) containing the peptide. After reaction at room temperature for 4 h, a solution of *N*-acetylcysteine (Sigma) was added to react with free maleimide groups. The resulting product was then purified by reverse-phase HPLC on a C4 column (Vydac) at 60 °C.

Cy7 was conjugated via a peptide bond to DSPE-PEG_{2000}-amine by adding a 3-fold molar excess of Cy7 mono-*N*-hydroxysuccinimide ester to the lipid dissolved in 10 mM aqueous sodium carbonate buffer (pH 8.5) containing 10% methanol by volume. After reaction at 4 °C for 8 h, the mixture was purified by HPLC as above.

Mixtures of fluorophore and peptide-containing DSPE-PEG_{2000} amphiphiles were prepared in a glass culture tube by dissolving each pure component in methanol, mixing the components, and evaporating the mixed solution under nitrogen. The resulting film was dried under vacuum for 8 h, then hydrated at 80 °C in water with a salt concentration of 10 mM NaCl. Samples were incubated at 80 °C for 30 min and allowed to cool to room temperature for 60 min. Solutions were then filtered through a 220-nm poly(vinylidene difluoride) syringe filter (Fisher Scientific).

Micelle Size as Determined by Dynamic Light Scattering (DLS). The presence of small spheroidal micelles was confirmed by particle size measurements using DLS. The DLS system (Brookhaven Instruments) consisted of an avalanche photodiode detector to measure scattering intensity from a 632.8-nm HeNe laser (Melles Griot) as a function of delay time. A goniometer was used to vary measurement angle, and consequently, the scattering wave vector, $\mathbf{q}$.

The first cumulant, Γ, of the first-order autocorrelation function, was measured as a function of scattering wave vector in the range 0.015–0.025 nm^{-1}. The quantity $\Gamma/\mathbf{q}^2$ was linearly extrapolated to $\mathbf{q} = 0$ to determine the translational diffusion coefficient of the aggregate, and the Stokes–Einstein relationship was used to estimate the micelle hydrodynamic diameter based on the measured diffusion coefficient.

Half-Life of Micelles in Circulation. The half-life of FAM-CREKA micelles and FAM-CREKA/Cy7/hirulog mixed micelles in circulation was determined by injecting 100 μL of 1 mM solution of micelles into BALB/c wild-type mice intravenously. Blood was collected from the retro-orbital sinus with heparinized capillary tubes from the same mouse at various times after injection. The blood was centrifuged at 1,000 $\times$ *g* for 2 min, and a 10-μL aliquot of plasma was diluted to 100 μL with PBS. Fluorescence of the plasma was measured by using a fluorimeter at an excitation wavelength of 485 nm and emission wavelength of 528 nm.

Targeting of Micelles to Atherosclerotic Plaques. Transgenic mice homozygous for the *Apoe*^{tm1Unc} mutation (The Jackson Laboratory) were fed a high-fat diet (42% fat, TD88137; Harlan) for 6 months to generate stage V lesions (24) in the brachiocephalic artery and aortic arch. Mice were housed, and all procedures were performed according to standards of the University of California, Santa Barbara, Institutional Animal Care and Use Committee. The mice were injected intravenously through the tail vein with 100 μL of 1 mM micelles containing either FAM-CREKA or a 1:1 mix of FAM and *N*-acetylcysteine as head groups. Micelles were allowed to circulate in the mice for 3 h, and the mice were then perfused with ice-cold DMEM through the left ventricle to remove any unbound micelles. The heart, aortic tree, liver, spleen, lungs, and kidneys were excised and fixed with 4% paraformaldehyde overnight at 4 °C. Ex vivo imaging was performed using a 530-nm viewing filter, Illumatool light source (Light Tools Research), and a Canon XTi DSLR camera. Tissue was then treated with a 30% sucrose solution for 8 h and frozen in OCT for cryosectioning. Quantification of fluorescence intensity was performed by using Image J software.

Thrombelastography Assay. A haemoscope thrombelastograph was used to assess the clotting properties of all materials investigated. This instrument provides quantitative data regarding time until clot initiation (*R*), rate of clot formation (Alpha), and strength of the clot formed (MA) by measuring the torsion of a small sample of blood around a wire during coagulation. First, 20 μL of 0.2 M $CaCl_2$ and the desired quantity of sample (micelles or iron oxide nanoparticles) were added to a plastic cup and heated to 37 °C. Next, 360 μL of plasma was added to the cup and the sample was loaded into position for commencement of the measurement.

Pooled human plasma in sodium citrate anticoagulant was purchased from George King Biomedical in 1-mL quantities. The samples were stored at −80 °C until 20 min before use, when they were heated to 37 °C in a water bath. Each vial of plasma was gently mixed immediately before use, and all samples were analyzed in plasma from the same lot number.

Tumor Targeting with CREKA Micelles. Orthotopic prostate cancer xenografts were generated by implanting 22Rv-1 (2×10^6 cells in 30 μL of PBS) human prostate cancer cells into the prostate gland of male nude mice. When tumor volumes reached ≈500 mm^3, the mice were injected with 100 μL of 1 mM FAM-CREKA micelles through the tail vein. The micelles were allowed to circulate for 3 h, and then mice were perfused through the left ventricle with ice-cold DMEM. The tumor was excised and frozen in OCT for sectioning.

Immunofluorescence. Serial cross-sections 5 μm thick of the brachiocephalic artery, aortic arch, healthy vessel, control organs, or 22Rv-1 prostate tumor were mounted on silane-treated microscope slides (Scientific Device Laboratory) and allowed to air dry. Sections were fixed in ice-cold acetone for 5 min and then blocked with Image-iT FX signal enhancer (Invitrogen). Alexa Fluor 647-conjugated rat anti-mouse antibodies to CD31 and CD68 (AbD Serotech) were used to visualize endothelial cells and macrophages and other lymphocytes, respectively. Fibrin(ogen) was stained with a primary polyclonal antibody made in goat and Alexa Fluor 647-conjugated anti-goat secondary antibody (Invitrogen). Sections were costained with DAPI in ProLong Gold antifade mounting medium (Invitrogen). Images of the vessels were taken with a confocal microscope.

Quantification of Hirulog Activity at Plaque Surface. The mice were injected through the tail vein with 100 μL of 1 mM (total lipid content) mixed micelles containing FAM-CREKA, CREKA, Cy7, and hirulog as head groups in a 3:3:0.3:3.7 ratio, respectively. Micelles were allowed to circulate in the mice for 3 h, and then mice were perfused with ice-cold DMEM through the left ventricle to remove any unbound micelles. The aortic tree was excised and homogenized in 1 mL of normal human plasma with sodium citrate (US Biological). Hirulog antithrombin activity was then quantified by using an assay with the S-2366 chromogenic substrate (diaPharma). Aortic tissue in plasma was incubated at 37 °C with an excess of thrombin for 2 min. The chromogenic substrate, S-2366, was then added and cleavage of the substrate by thrombin, causing the release of *para*-nitroanaline was quantified by measuring absorbance at 405 nm. Higher concentrations of hirulog resulted in less cleavage of the substrate and lower absorbance values. A standard curve was used to convert the absorbance values to milligrams of hirulog.

ACKNOWLEDGMENTS. We thank Dr. Lilach Agemy for the 22Rv1 mouse prostate tumor model, April Saywel for performing the thrombelastography assay, and Peter Allen for the micelle graphic. This work was supported by National Heart, Lung, and Blood Institute Program of Excellence in Nanotechnology Grant HL070818, and, in part, by the National Center for Research Resources Shared Instrumentation Grant 1S10RR017753 and Materials Research Science and Engineering Centers Program of the National Science Foundation Award DMR05-20415.

1. Rosamond W, et al. (2007) Heart disease and stroke statistics–2007 update: A report from the American Heart Association Statistics Committee and Stroke Statistics Subcommittee. *Circulation* 115:e69–e171.
2. Davies MJ (1992) Anatomic features in victims of sudden coronary death. Coronary artery pathology. *Circulation* 85:I19–I24.
3. Ghigliotti G, Waissbluth AR, Speidel C, Abendschein DR, Eisenberg PR (1998) Prolonged activation of prothrombin on the vascular wall after arterial injury. *Arterioscler Thromb Vasc Biol* 18:250–257.
4. Ivey ME, Little PJ (2008) Thrombin regulates vascular smooth muscle cell proteoglycan synthesis via PAR-1 and multiple downstream signalling pathways. *Thromb Res* 123:288–297.
5. Duguid JB (1946) Thrombosis as a factor in the pathogenesis of coronary atherosclerosis. *J Pathol Bacterial* 58:207–212.
6. Duguid JB (1948) Thrombosis as a factor in the pathogenesis of aortic atherosclerosis. *J Pathol Bacteriol* 60:57–61.
7. Smith EB (1993) Fibrinogen and atherosclerosis. *Wien Klin Wochenschr* 105:417–424.
8. Alonso A, et al. (2007) Molecular imaging of human thrombus with novel abciximab immunobubbles and ultrasound. *Stroke* 38:1508–1514.
9. Bode C, et al. (1994) Fibrin-targeted recombinant hirudin inhibits fibrin deposition on experimental clots more efficiently than recombinant hirudin. *Circulation* 90:1956–1963.
10. Stoll P, et al. (2007) Targeting ligand-induced binding sites on GPIIb/IIIa via single-chain antibody allows effective anticoagulation without bleeding time prolongation. *Arterioscler Thromb Vasc Biol* 27:1206–1212.
11. Houston P, Goodman J, Lewis A, Campbell CJ, Braddock M (2001) Homing markers for atherosclerosis: Applications for drug delivery, gene delivery and vascular imaging. *FEBS Lett* 492:73–77.
12. Liu C, Bhattacharjee G, Boisvert W, Dilley R, Edgington T (2003) In vivo interrogation of the molecular display of atherosclerotic lesion surfaces. *Am J Pathol* 163:1859–1871.
13. Briley-Saebo KC, et al. (2008) Targeted molecular probes for imaging atherosclerotic lesions with magnetic resonance using antibodies that recognize oxidation-specific epitopes. *Circulation* 117:3206–3215.
14. Karmali PP, et al. (2008) Targeting of albumin-embedded paclitaxel nanoparticles to tumors. *Nanomedicine* 5:73–82.
15. Kelly KA, Nahrendorf M, Yu AM, Reynolds F, Weissleder R (2006) In vivo phage display selection yields atherosclerotic plaque targeted peptides for imaging. *Mol Imaging Biol* 8:201–207.
16. Simberg D, et al. (2007) Biomimetic amplification of nanoparticle homing to tumors. *Proc Natl Acad Sci USA* 104:932–936.
17. Nakashima Y, Plump AS, Raines EW, Breslow JL, Ross R (1994) ApoE-deficient mice develop lesions of all phases of atherosclerosis throughout the arterial tree. *Arterioscler Thromb* 14:133–140.
18. Reddick RL, Zhang SH, Maeda N (1994) Atherosclerosis in mice lacking apo E. Evaluation of lesional development and progression. *Arterioscler Thromb* 14:141–147.
19. Eitzman DT, Westrick RJ, Xu Z, Tyson J, Ginsburg D (2000) Plasminogen activator inhibitor-1 deficiency protects against atherosclerosis progression in the mouse carotid artery. *Blood* 96:4212–4215.
20. Maeda N, et al. (2007) Anatomical differences and atherosclerosis in apolipoprotein E-deficient mice with 129/SvEv and C57BL/6 genetic backgrounds. *Atherosclerosis* 195:75–82.
21. Falk E, Schwartz SM, Galis ZS, Rosenfeld ME (2007) Putative murine models of plaque rupture. *Arterioscler Thromb Vasc Biol* 27:969–972.
22. Richardson PD, Davies MJ, Born GV (1989) Influence of plaque configuration and stress distribution on fissuring of coronary atherosclerotic plaques. *Lancet* 2:941–944.
23. Maraganore JM, Bourdon P, Jablonski J, Ramachandran KL, Fenton JW, II (1990) Design and characterization of hirulogs: A novel class of bivalent peptide inhibitors of thrombin. *Biochemistry* 29:7095–7101.
24. Whitman SC (2004) A practical approach to using mice in atherosclerosis research. *Clin Biochem Rev* 25:81–93.